Behaviour of (U,Am)O_2 in oxidizing conditions: a high-temperature XRD study

E. Epifano, R. Vauchy, F. Lebreton, A. Joly, C. Guéneau, Ch. Valot, P.M. Martin

Behaviour of $(U,Am)O_2$ in oxidizing conditions: a high-temperature XRD study.

E. Epifano,[†] R. Vauchy,[†] F. Lebreton,[†] A. Joly,[†] C. Guéneau,[‡] Ch. Valot,[†] and P. M. Martin[*,†]

†*CEA, DEN, DMRC, Univ Montpellier, Marcoule, France*

‡*DEN-Service de Corrosion et du Comportement des Matériaux dans leur Environnement (SCCME), CEA, Université Paris-Saclay, F-91191 Gif-sur-Yvette, France*

E-mail: enrica.epifano@onera.fr

Abstract

Uranium-Americium oxides $U_{1-y}Am_yO_{2\pm x}$ are currently investigated as possible transmutation targets for next generation nuclear reactors. In the context of a comprehensive investigation of the thermodynamic and thermal properties of these materials, their behaviour in oxidizing conditions is here investigated for the first time. The results of high-temperature X-ray diffraction measurements in air are here presented. A wide composition domain of the solid solution has been investigated, measuring $U_{1-y}Am_yO_{2\pm x}$ oxides with Am/(Am+U) ratios ranging from 0.10 to 0.67. This allowed determining the effect of the americium content on the oxidation kinetics in air. Specifically, it will be shown that americium hinders the formation of the M_4O_9 and M_3O_8 phases.

1 Introduction

In the frame of the transmutation of minor actinides, uranium-americium mixed dioxide $U_{1-y}Am_yO_{2\pm x}$ are promising targets for generation-IV nuclear reactors[1] and they have recently been the subjects of various studies. The design of fast neutron reactors include hypo-stoichiometric dioxide fuel, i.e. MO_{2-x}, in order to limit the interaction with the cladding.[2–5] It is hence logical that the first investigations on $U_{1-y}Am_yO_{2\pm x}$ oxides have focused on the oxygen hypo-stoichiometric domain.[6–12] However, in order to assure the safety of reactors both in normal and accidental conditions, a comprehensive knowledge of the thermal and thermodynamic properties of the materials present in the reactor is necessary. Up to now, very few data exist on uranium-americium mixed oxides with oxygen/metal ratio (O/M) higher than 2. Indeed, only three studies report data on the oxygen-rich domain of the $U_{1-y}Am_yO_{2\pm x}$ solid solution. The first concerns the oxygen potential measurements performed on $U_{0.5}Am_{0.5}O_{2\pm x}$ by Bartscher and Sari;[13] these data indicate that the fluorite-type solid solution can reach O/M values of about 2.09, for $973 \leq T \leq 1573$ K and $-60 \leq \Delta\overline{G}O_2 \leq -7$ kJ/mol. The second is a recent investigation, by Caisso *et al.*,[14] that indicates a small solubility (Am/M=10 at.%) of americium in the hexagonal $\alpha' M_3O_8$ structure (s.g. P-62m). Finally, some melting temperature measurements were performed in air on $U_{0.5}Am_{0.5}O_{2\pm x}$ oxides, whose final O/M were higher than 2.0.[15] However, no data exist on the transition temperatures and the phase limits in the MO_2-M_4O_9-M_3O_8 domain. These features are hard to predict since the binary systems U-O and Am-O present different phase diagrams and they have very different behaviours in oxidizing conditions. The U-O phase diagram includes several oxides with O/M>2, namely U_4O_9, metastable U_3O_7, U_3O_8 and UO_3.[16] Several studies are available on the oxygen-rich domain of the U-O phase diagram and on the oxidation process in air.[17–20] High-Temperature X-ray Diffraction (HT-XRD) measurements on UO_2 showed that the dioxide, in air, is quickly oxidized to U_4O_9 for $T > 473$ K.[21] Subsequently, the $U_4O_9 \rightarrow U_3O_8$ phase transition occurs at $T = 673$ K. Once formed, the U_3O_8 phase, with its different polymorphs, is stable in air, up to 1673 K and, during the subsequent cooling,

untill room temperature. AmO_2 is the americium oxide with the highest O/M ratio and it behaves in air in a very different way than UO_2: when heated, AmO_2 not only maintains its fluorite structure, but it also starts to be reduced (O/M<2) for T > 1200 K.[22]

Thus, the pronounced differences between the Am-O and the U-O phase diagrams lead to a completely different behaviour of the respective dioxides in air. It is hence difficult to infer information about the oxygen rich domain of the ternary U-Am-O phase diagram and the behaviour of (U,Am)O_2 oxides in oxidizing conditions, especially because various studies have shown that they do not exhibit an ideal solid solution behaviour.[7,9,12,15] For this reason, an investigation by High-Temperature X-ray Diffraction (HT-XRD) over a wide compositional domain is here presented. The effects of the americium addition to UO_2 on the oxidation kinetics will be shown and the solubility of americium in M_3O_8 will be inferred from the crystallographic data.

2 Experiment

2.1 Materials

$U_{1-y}Am_yO_{2\pm x}$ oxides with nominal americium content y = 0.10, 0.15, 0.30, 0.50 and 0.70 were synthesized for this study, each one identified herein with the reference indicated in Tab. 1. The samples were initially manufactured as form of pellets in the Atalante facility of CEA Marcoule, using as precursors UO_2 and AmO_2 powders. The former was depleted uranium dioxide, whose total content of impurities was below 100 ppm. The O/U ratio was measured by polagraphy and it was equal to 2.04. The AmO_2 batch came from a test of liquid-liquid extraction from spent fuel with the EXAM process[23] and it presented some percent of impurities, mainly Ce (1.7(5) wt.%), Nd (0.5(1) wt.%) and Np (0.4 wt.%). The O/M ratio could not be directly measured, but a thermal treatment in dry air was performed on the AmO_2 powder, at 673 K for 12 hours, which is considered sufficient to establish the stoichiometry O/Am = 2.0.[22] The precursor powders were mixed, ground by ball-milling and

pressed into pellets of about 500-700 mg. The UMACS powder metallurgy process[24] was applied for the synthesis of the mixed oxides. This process includes two thermal treatments-with intermediate grinding and pelletization- performed in a tungsten furnace, with plateau temperatures of 2023 K, for Am/M $\leq$ 30 mol.%, and 1873 K for higher Am concentrations. For the atmosphere, a flowing mixture of Ar/H_2(4%) and Ar/O_2(1000 ppm) was used, in order to obtain oxygen potentials of about -450 kJ/mol at 2023 K and -440 kJ/mol at 1873 K. The obtained pellets were ground in an agate mortar and the powder characterized by XRD, thermal ionization mass spectrometry (TIMS) and XAS. TIMS allowed determining the obtained Am/(Am+U) ratio of the samples. The XRD patterns of all the compositions confirmed the presence of one single fluorite-type phase, indicating that the formation of the solid solution was achieved. XAS was performed on a few mg of powder for the compositions investigated in this work, at the Rossendorf beamline of the ESRF (Grenoble, France). The L_3 edges of U and Am were probed and the spectra were compared to those obtained on reference materials (UO_2, U_4O_9, U_3O_8, AmO_2 and an oxalate with Am^{3+}). This allowed determining the average oxidation states of U and Am. Then, from the electroneutrality rule, the O/M ratios were obtained. The results of the XAS study on the as-sintered oxides are published in a previous work.[12] The compositions of the samples are summarized in Tab. 1.

Table 1: Compositions of the samples

Reference	Am/(Am+U) (at.%)	O/M ratio
Am10	10(1)	2.01(2)
Am15	15(2)	2.02(2)
Am30	28(2)	2.02(2)
Am50	48(1)	1.97(2)
Am70	67(3)	1.90(2)

The samples were stored for about 7 months before the measurements, with the exception of the Am10 sample which was annealed in argon before the HT-XRD experiment. The annealing treatment was initially planned for all the samples but it could no be performed for technical problems. For each composition, between 20-40 mg of powder were used during

the HT-XRD measurements.

2.2 Experimental set-up and procedure

HT-XRD measurements were performed at the LEFCA facility of CEA/Cadarache (France) with a Bragg-Brentano $\theta - \theta$ Bruker D8 Advance X-ray diffractometer using Cu radiation from a conventional tube source ($K_{\alpha 1}+K_{\alpha 2}$ radiation: $\lambda = 1.5406$ and 1.5444 Å). The device, implemented in a glovebox dedicated to nuclear materials, was described in previous works.[25] A MRI-Hightemp hot stage was used for heating the sample. The furnace allows heating the sample up to 2273 K using a metallic strip and a radiant heater, both made of Mo or a platinum-rhodium alloy. In this work, considering the oxidizing atmosphere, the PtRh strip was preferred. Before the measurements, a temperature calibration was carried out in steps of 100 K from room temperature up to 1873 K using MgO powder as reference. According to previous experiments, a constant uncertainty of $\pm$ 15 K is estimated on the temperature range considered. The atmosphere inside the hot stage was controlled through a constantly flowing gas of purified air. All the studied compositions underwent the same thermal treatment in air. They were heated from 300 K up to about 1470 K, with temperature steps of 50 K. At each step, a diffraction pattern in the $18° \leq 2\theta \leq 140°$ range was acquired. One acquisition requires about 30 minutes. The heating rate between the steps was 5 K/s. At the end of the heating stage, a plateau of 4 hours was performed at the maximum temperature. Finally, the sample was cooled down recording a diffraction pattern every 100 K. A cooling rate of 5 K/s was applied between the steps. XRD patterns refinement was performed according to the Pawley method[26] or the Rietveld method[27] (specified in the following case by case) using the TOPAS 4.0 software.[28]

3 Results

3.1 General evolution in air

An overview of the behaviour in air of the $U_{1-y}Am_yO_{2\pm x}$ oxides is provided in Fig. 1, where isointensity maps were created from the diffraction patterns, recorded at different temperatures. Both the heating and the cooling stages are included in the representation. The specific angular range was selected because it includes intense diffraction peaks of all the observed phases.

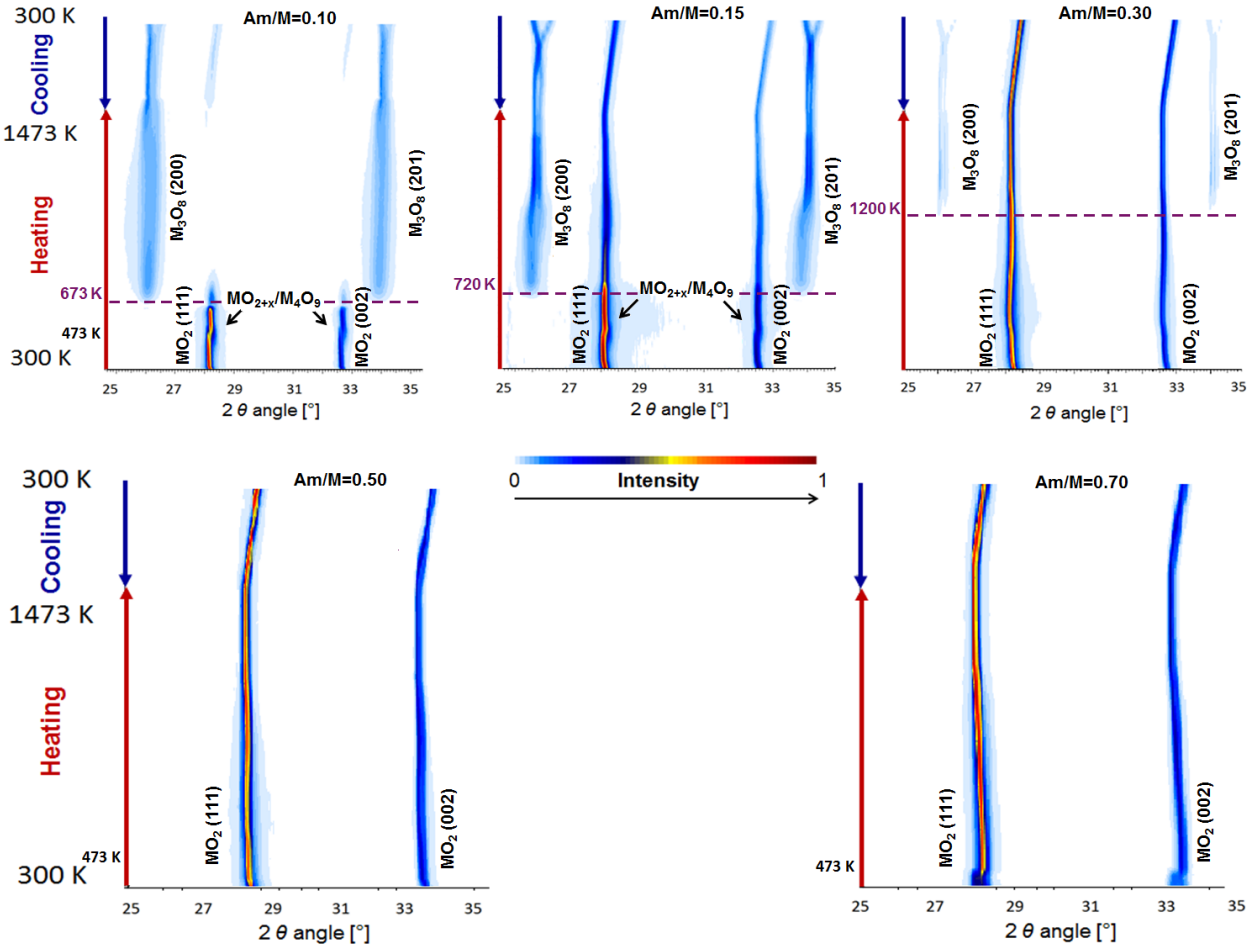

Figure 1: Iso-intensity map of HT-XRD measurements in air on Am10, Am15, Am30, Am50 and Am70 (from left to right and from top to bottom).

Two different behaviours can be identified: the oxides with Am/(Am+U) $\leq$ 0.30 undergo

a phase transition during the heating in air, whereas the Am/(Am+U) = 0.50 and 0.70 show a single fluorite phase during the entire heat treatment. The latter two exhibit hence a behaviour in air similar to AmO_2 and this will be further discussed in the next section, considering the lattice parameter expansion.

Focusing now on the iso-intensity maps of the former three compositions, one can observe that distortions of the cubic structure reflections are observable during heating, for temperature higher than 473 K. These correspond to variations of the lattice cell parameter, which can be caused by several factors, such as thermal expansion, O/M variation, annealing of defects. The most evident shifts and distortions were observed for Am10 and Am15 and they are similar to those that can be observed for UO_2.[21] This likely indicates the formation of the fluorite-related M_4O_9 phase. It must be observed that, since the solubility of Am in U_4O_9 and U_3O_8 is unknown, one cannot trivially conclude on the repartition of americium between the phases. Therefore, in the biphasic region, the Am/(Am+U) ratio of each phase is unknown. Consequently, in the following, the phases will be indicated as "MO_2", "M_4O_9" and "M_3O_8", where M = Am, U.

Going to higher temperatures, a second phase appeared and subsequently the two phases coexisted for the rest of the measurement, during both heating and cooling. The additional diffraction peaks correspond to the hexagonal structure (s.g. P-62m, N° 189) of α'-U_3O_8.[29] Interestingly, the appearance of the M_3O_8 phase was shifted to higher temperatures by increasing the total amount of americium. Moreover, strong differences were observable for the MO_2/M_3O_8 relative intensities between the three samples: the higher the americium content, the lower the M_3O_8/MO_2 intensity ratio.

3.2 Evolution of the cubic phase and phase transitions

The XRD patterns acquired during the thermal treatments in air were refined according to the Pawely method.[26] For the cubic phase, the *Fm-3m* structure was always used. However, the adoption of the fluorite-related M_4O_9 superstructure (4x4x4 fluorite cells)[30] give similar

results for the fit of XRD patterns. The *Fm-3m* structure was preferred in order to directly compare all the cubic lattice parameters. Indeed, the lattice parameter variations of the cubic phase can be directly related to its composition changes and these will be detailed in the following for each oxide.

Am10. As previously mentioned, the Am10 sample was thermally treated at 1273 K in $Ar/H_2(5\%)$ for 4 hours, in order to anneal the defects induced by the self-irradiation, before the HT-XRD experiment. The oxide was about 3 hours old when the first XRD pattern was recorded at room temperature. The corresponding lattice parameter was $a = 5.464(1)$ Å. The variation in the lattice parameter as a function of temperature is represented in Fig. 2-(a). The data of both the heating (red) and the cooling (blue) steps are shown. On the right side of the figures, portions of the XRD patterns for selected temperatures are also reported. The

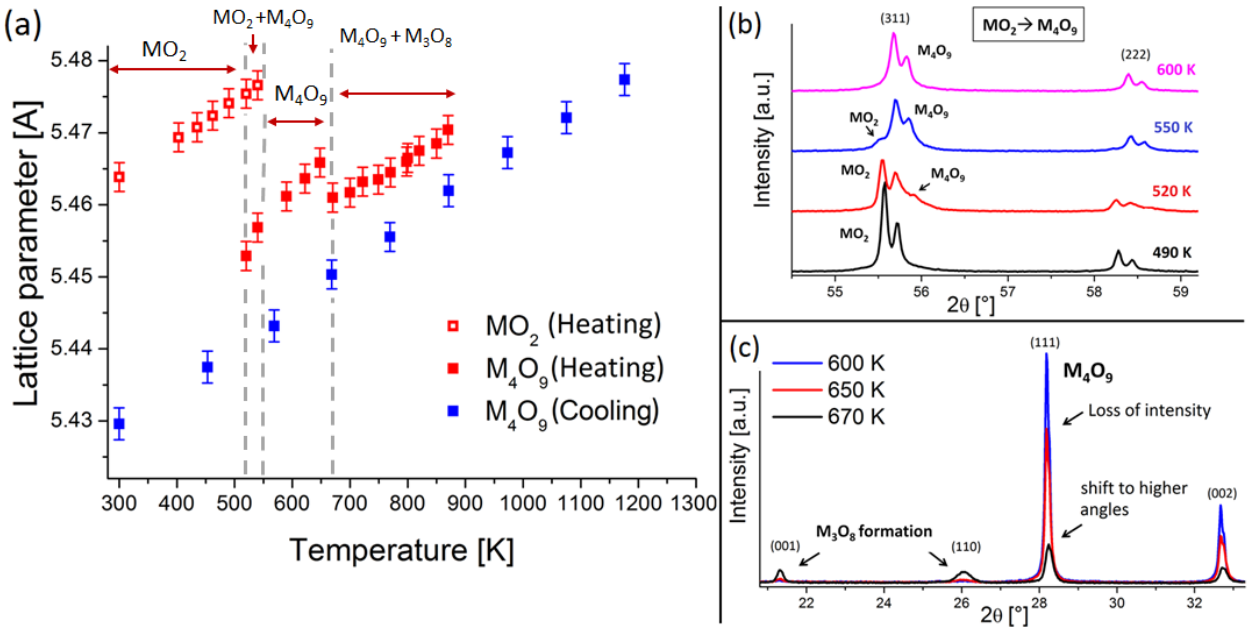

Figure 2: Behaviour of the Am10 sample in air: (a) evolution of the lattice parameter of the cubic structure as a function of the temperature; (b) excerpts of the XRD patterns, for selected temperatures, showing the (311) and (222) reflections of the *Fm-3m* structure during heating; (c) extracts of the XRD patterns, for selected temperatures, showing the (111), (002) reflections of the *Fm-3m* structure and the (001) (110) reflections of the *P-62m* structure.

variation of the lattice parameter highlights several sequences during the thermal treatment in air. A possible composition-temperature path is represented on the U-O phase diagram, in Fig. 4 (red path), and compared to the UO_2 evolution in air descibred by Chollet *et al.*[21] (grey path). The represented phase diagram domain is a modified version (unpublished) of the Gueneau,[16] where the composition ranges of the U_4O_9 and U_3O_8 are represented. The reaction path was traced as a guide for the eye only; it must be stressed that this is a simplified representation since it does not take into account the effect of americium on the phase equilibria.

For Am10, at the beginning of the heating, from 300 to 490 K, an approximately linear expansion of the lattice parameter occurred for the MO_2 phase, as shown in Fig. 2-(a). At T = 520 K, a second cubic structure appeared. This is shown in Fig. 2-(b), where portions of the XRD pattern are reported. A shoulder at higher angle was present on the (311) reflection of the MO_2 phase (the shoulder is indicated by an arrow; it should not be confused with the double peak, which is observed for all the reflection conditions, due to the two wavelengths of the copper source, Cu Kα_1 and Cu Kα_2). The lattice parameter of the second cubic phase was much smaller than the previous one (5.453 Å vs 5.475 Å at 520 K). The only phenomenon that can explain this difference is a considerable increase in the O/M ratio, since the self-irradiation defects were previously annealed. Indeed, it is well established that, in fluorite-type oxides, the lattice parameter decreases when the O/M increases, and *vice versa*. The second cubic structure can hence be associated to the M_4O_9 phase. The M_4O_9 rapidly became the most intense and, at 600 K, the MO_2 completely disappeared. Subsequently to its formation, a regular thermal expansion of the M_4O_9 phase was observed in the $520 \leq T \leq 648$ K temperature range. At T = 670 K, another discontinuity of the lattice parameter was observed. This corresponded to the appearance of the M_3O_8 phase, as shown by the portions of XRD patterns in Fig. 2-(c). However, if the loss of intensity in the cubic reflections is clearly explained by the M_3O_8 appearance, their shift to higher angles (XRD pattern at 670 K) and the corresponding decrease in the lattice parameter cannot be simply explained

by the formation of the new structure. They indicate a composition change in the cubic phase, most likely an enrichment in americium. This implies that the Am/(Am+U) ratios were not equal in the two co-existing phases and that the solubility of americium in M_3O_8 structure was lower than Am/M=10 at.% at that temperature. Continuing the heating, another approximately regular expansion of the M_4O_9 lattice parameter was observed up to 870 K, meanwhile the intensity of the M_3O_8 reflection was increasing. Above 870 K, the hexagonal phase was the most intense. As shown in Fig. 3, at 1470 K, the M_4O_9 reflections were barely visible (for this reason, the lattice parameter of this phase could not be obtained in the high-temperature range). No evolution of the diffraction pattern was observed during the 4-hours dwell at this temperature.

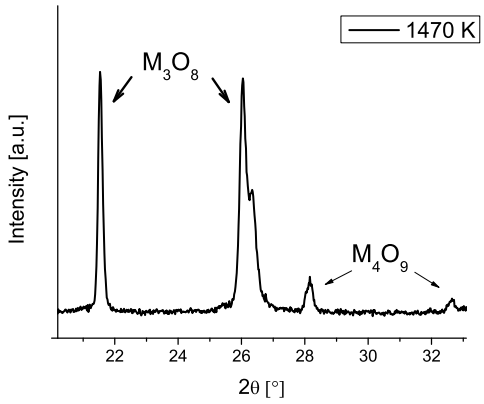

Figure 3: XRD patter acquired at 1470 K on the Am10 sample, in air.

One must be careful before concluding on the relative phase fractions at high temperature. Indeed, the formation of M_3O_8, whose density is lower than MO_2 (ρ_{UO_2}= 10.95 g/cm^3, $\rho_{U_3O_8} \simeq$ 8.3 g/cm^3 [31]), leads to a swelling of the sample. This causes irregularities in the surface of the powder, hence the X-ray absorption could reduce the intensity of low angle peaks. The amount of M_4O_9 cannot be clearly quantified. The diffraction peaks of the cubic phase were more intense during cooling, for T $<$ 1172 K. In this range, the lattice parameters could be determined and the observed variation was regular untill room temperature. This indicates a mostly constant composition during cooling. The final lattice parameter at

room temperature was 5.430(3) Å. The value is considerably smaller than the initial one, confirming the increase in the O/M ratio. A phase transition was observed for the M_3O_8 phase during cooling. As shown in Fig. 4, the stable U_3O_8 form at high temperature (T > 570 K) is the hexagonal α' (*P-62m*). For lower temperatures, the β (*Cmcm*) and α (*C2mm*) polymorphs, both orthorombic, appear. For the Am/(Am+U) = 0.10 sample, a structural change from hexagonal to orthorombic was observed at about 570 K, as shown in Fig. 5. The XRD patterns can be differentiated through the doubling of the reflection at about 26°.

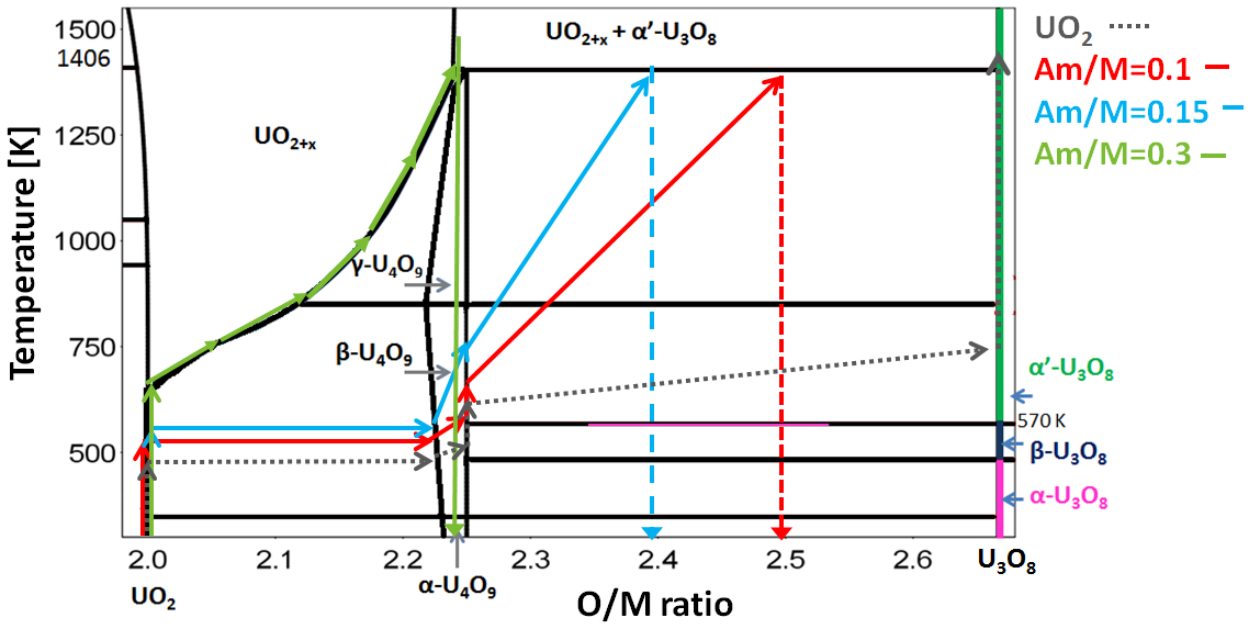

Figure 4: Qualitative representation of the composition-T paths during the heating under air.

Am15. The initial lattice parameter of Am15 at room temperature was equal to 5.476(1) Å, hence considerably larger than that of Am10. The difference is due to the α self-irradiation. The value represents a swelling of 0.27% relatively to the defect-free lattice parameter, $a_0 = 5.461(1)$ Å,[32] which was consistent with the age of the sample of 220 days. The variation in the cubic lattice parameter during the thermal treatment is shown in Fig. 6. A possible composition-temperature path is represented in Fig. 4 with a blue line. From 300 to 535 K, an almost linear increase of the cubic lattice parameter occurred, as shown in

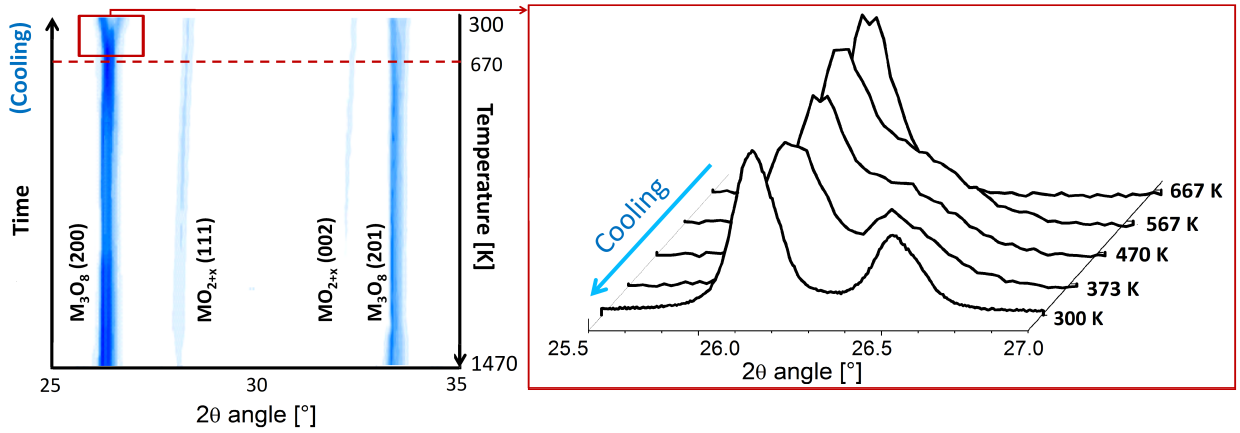

Figure 5: Cooling in air of the Am10 sample: zoom on the $25.5<2\theta<27°$ range of the XRD patterns. The doubling of the XRD peak indicates the transition from the hexagonal *P-62m* to the orthorombic *C2mm* structure for M_3O_8.

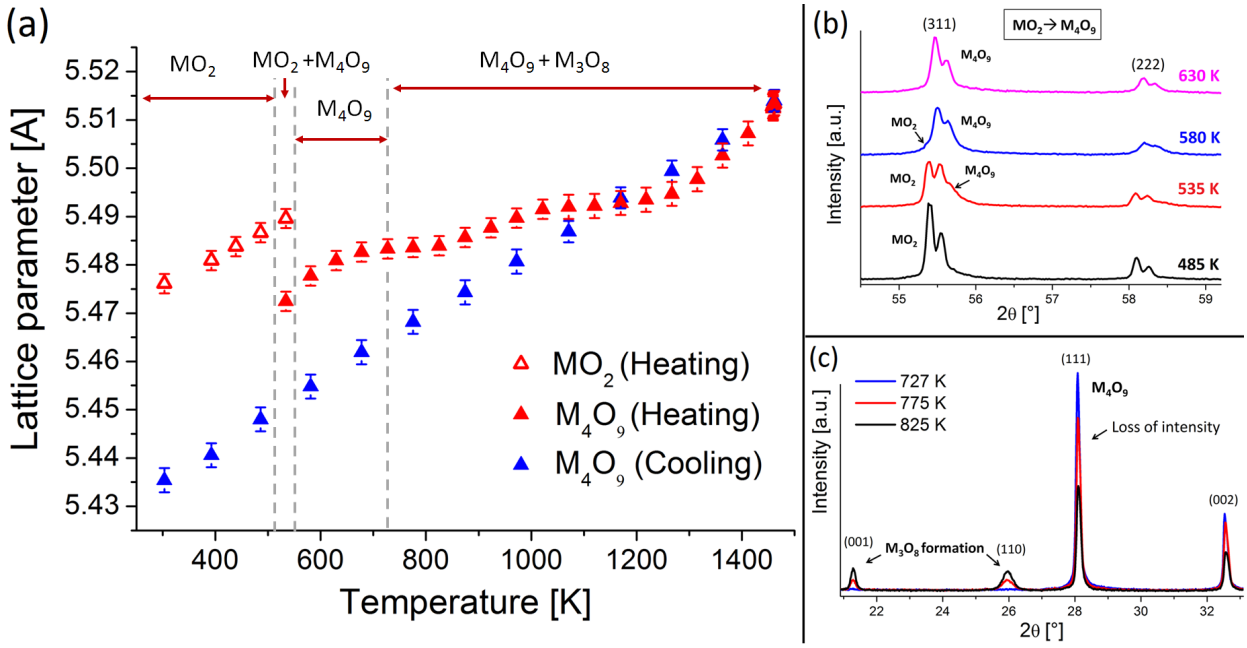

Figure 6: Behaviour of the Am15 sample in air:(a) evolution of the lattice parameter of the cubic structure as a function of the temperature; (b) extracts of the XRD patterns, for selected temperatures, showing the (311) and (222) reflections of the Fm-3m structure; (c) extracts of the XRD patterns, for selected temperatures, showing the (111), (002) reflections of the Fm-3m structure and the (001) (110) reflections of the P-62m structure.

Fig. 6-(a). A second cubic structure appeared at about 535 K, as shown in Fig. 6-(b). Similarly to Am10, the lattice parameter of the second cubic phase was considerably smaller than the first one: 5.472(2) Å versus 5.490(2) Å at 535 K. In this case, contrarily to the Am10

sample, the annealing of defects has likely contributed to the decrease of the lattice parameter. However, the determined contraction is of about 0.33% and hence it cannot be due only to the recovering from self-irradiation (previously determined at 0.27%). The difference can be explained only by an increase of the O/M ratio. Moreover, the brief co-existence of two FCC structures with different O/M ratios leads again to the identification of the second cubic structure with the M_4O_9 phase. This rapidly became the most abundant phase and, at 630 K, MO_2 had completely disappeared. An increase of the M_4O_9 lattice parameter was observed for $535 < T < 727$ K. However, this thermal expansion is not linear and it seems slowed down in comparison to the previous one observed for Am10. This indicates the occuring of another phenomenon contrasting the thermal expansion, which can likely be attributed to an increase of the O/M ratio. Therefore, a crossing of the oxygen composition domain of the M_4O_9 phase can be supposed, as schematically shown in the scheme in Fig. 4. Subsequently, at T=727 K, the M_3O_8 phase appeared, as shown in Fig. 6-(c). A corresponding slope break was observed in the variation of the M_4O_9 lattice parameter (Fig. 6-(a)). This indicates a change in its composition, which can be associated to a redistribution of the U and Am species between the two phases. This continued up to about 1267 K. Above this temperature, the increase of the M_4O_9 lattice parameter becomes linear. Contrary to the Am10 sample, the M_4O_9 was clearly visible in the XRD patterns during the entire thermal treatment. Moreover, comparing the lattice parameter variations of the two samples, it can be seen that the appearance of M_3O_8 occurred in a smoother way for Am15 rather than for Am10. These data indicate that the overall increase in the O/M ratio of Am15 is likely lower than that of Am10, for which the oxidation is abrupter, likely because the final O/M was quite far from the initial one.

At the highest temperature (1470 K), the lattice parameter was constant at 5.513(3) Å during the 4 hours plateau and no evident evolution of the XRD pattern was observed. This indicates that the oxide was likely in thermodynamic equilibrium. Then, a regular linear decrease of the M_4O_9 lattice parameter was observed during cooling, indicating a mostly

constant composition for the entire temperature range. The final lattice parameter at room temperature was 5.434(2) Å. The value is considerably smaller than the initial one and also of the defect-free lattice parameter of a $U_{0.85}Am_{0.15}O_2$ oxide, which is 5.464(1) Å.[33] This confirms the increase of the O/M ratio and, possibly, the enrichment in americium of the cubic phase. As for Am10, the transition of the M_3O_8 phase from the hexagonal toward the orthorhombic form was observed during the cooling, at about 580 K, as shown in Fig. 7.

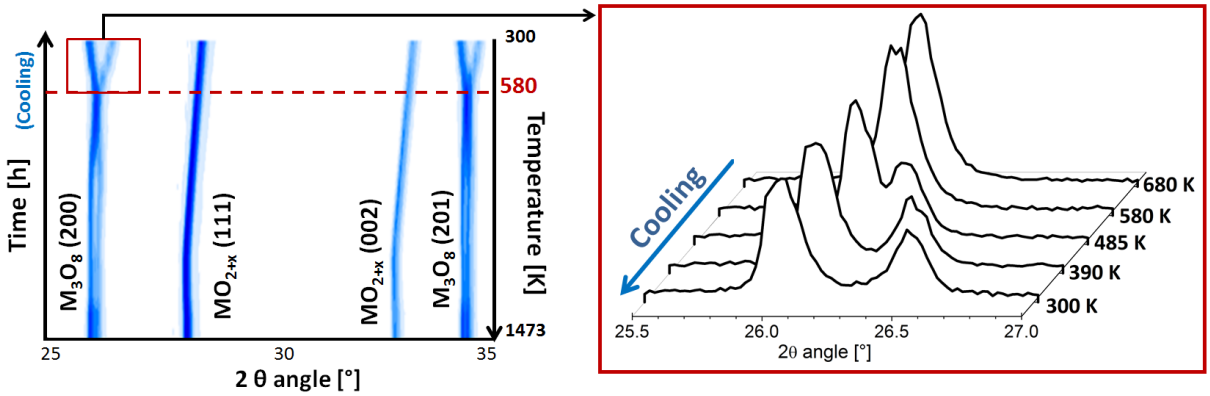

Figure 7: Cooling in air of Am15: isointensity map and zoom on the 25.5<2θ<27° range of the XRD patterns. The doubling of the XRD peak indicates the transition from the hexagonal *P-62m* to the orthorombic *C2mm* structure for M_3O_8.

Am30. The initial lattice parameter at room temperature of Am30 was equal to 5.468(1) Å. The value corresponds to a swelling of 0.275% relatively to the defect-free lattice parameter, a_0 = 5.453(1) Å, according to Lebreton.[33] The lattice parameter was consistent with the age of the sample of 210 days. The evolution of the cubic lattice parameter as a function of the temperature is shown in Fig. 8. A schematic composition-temperature path is represented by the green line in Fig. 4.

At the beginning of the thermal treatment, for T $\leq$ 650 K, an almost linear increase of the lattice parameter with the temperature is observed. In this range, a slight break of the slope is visible at about 464 K, likely due to the the annealing of the self-irradiation defects. For 650$\lesssim$ T $\lesssim$1000 K, the thermal expansion of the cubic phase was remarkably slowed down and almost constant lattice parameter values were observed. This indicates a

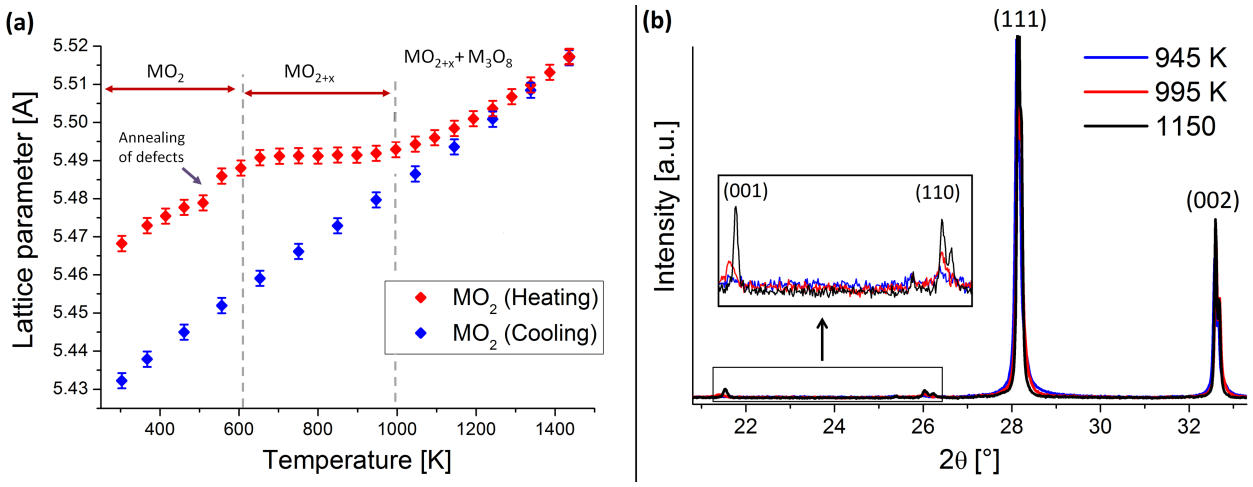

Figure 8: Behaviour of Am30 in air:(a) evolution of the lattice parameter of the cubic structure as a function of the temperature; (b) extracts of the XRD patterns, for selected temperatures (heating), showing the (111), (002) reflections of the Fm-3m structure and the (001) (110) reflections of the P-62m structure.

slow, continuous increase of the O/M ratio and hence this cubic structure is identified with the MO_{2+x} phase. At the end of the MO_{2+x} oxidation, at about 995 K, the first reflections of the M_3O_8 structure were observed, with very low intensity, as shown in Fig. 8-(b). Above 995 K, a linear increase of the MO_{2+x} lattice parameter with the temperature was observed up to 1473 K. At this temperature, the lattice parameter was constant at 5.517(2) Å during the 4 hours plateau and no evolution of the XRD pattern was observed, indicating that the thermodynamic equilibrium was likely achieved. During the entire cooling, a regular linear decrease of the MO_{2+x} lattice parameter was observed, indicating a mostly constant composition. The transition of the M_3O_8 phase from the hexagonal toward the orthorhombic form was observed during the cooling, for $480 < T < 556$ K, as shown in Fig. 9.

Am50 and Am70. The lattice parameters of the Am50 and Am70 samples, for both heating and cooling, are reported in Fig. 10.

The initial lattice parameter at room temperature of Am50 was $a = 5.466(1)$ Å. At the time of the measurement, 194 days had passed since the sintering of the sample. This period is longer than that necessary, for this composition, to reach the saturation of the self-irradiation

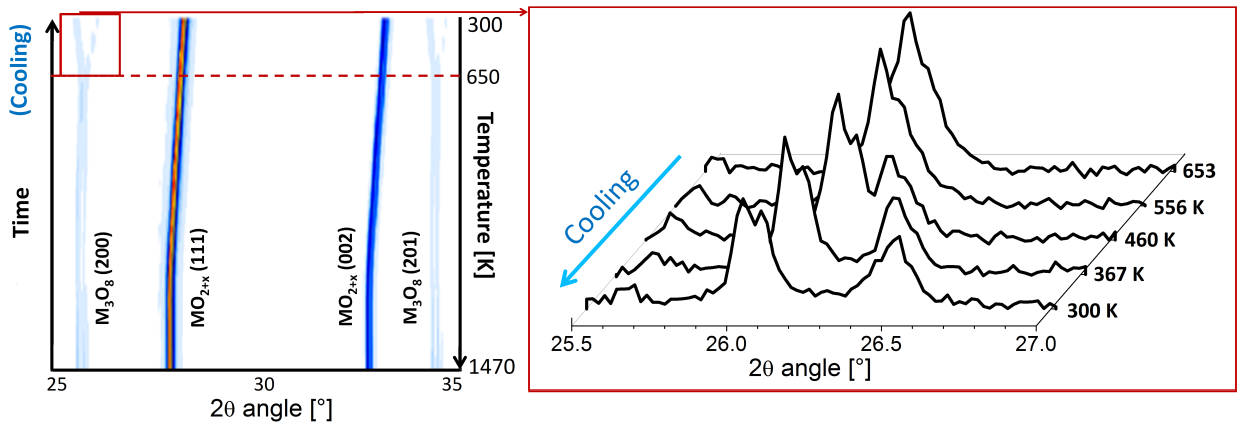

Figure 9: Cooling in air of Am30: zoom on the 25.5<2θ<27° range of the XRD patterns. The doubling of the XRD peak indicates the transition from the hexagonal *P-62m* to the orthorombic *C2mm* structure for M_3O_8.

swelling, corresponding to $a = 5.467(1)$ Å,[33] consistently with the measured value. For Am70, the lattice parameter at room temperature was $a = 5.450(1)$ Å. The sample was 190 days old at the time of the measurements and, as in the previous case, the swelling should have reached the saturation. The expected value was, according to Lebreton,[33] $a = 5.454(1)$ Å. The difference compared to the observed value is very small and it is likely due to slight differences in the Am/(U+Am) and O/M ratios between the sample of Lebreton[33] and that of this work. At the beginning of the heating, some differences can be remarked between the two compositions. For Am50, the lattice parameter increased with the temperature, but not in a regular way. More specifically, two slowdowns are observed: the first for $413 \lesssim T \lesssim 508$ K, the second for $750 \lesssim T \lesssim 950$ K. This evolution can be due to both annealing of defects and increase of the O/M ratio. Above 950 K, a linear increase of the lattice parameter was observed. For Am70, a decrease of the lattice parameter was observed at the beginning of the heating, likely due to the annealing of defects. Subsequently, a mostly linear increase of the lattice parameter was observed during the entire heating. For both the compositions, the lattices parameters were stable during the 4 hours plateau at 1473 K, at 5.521(2) Å and 5.506(2) Å, for Am/(Am+U)=0.5 and 0.7, respectively.

During the cooling, a regular linear decrease of the lattice parameter was observed for both

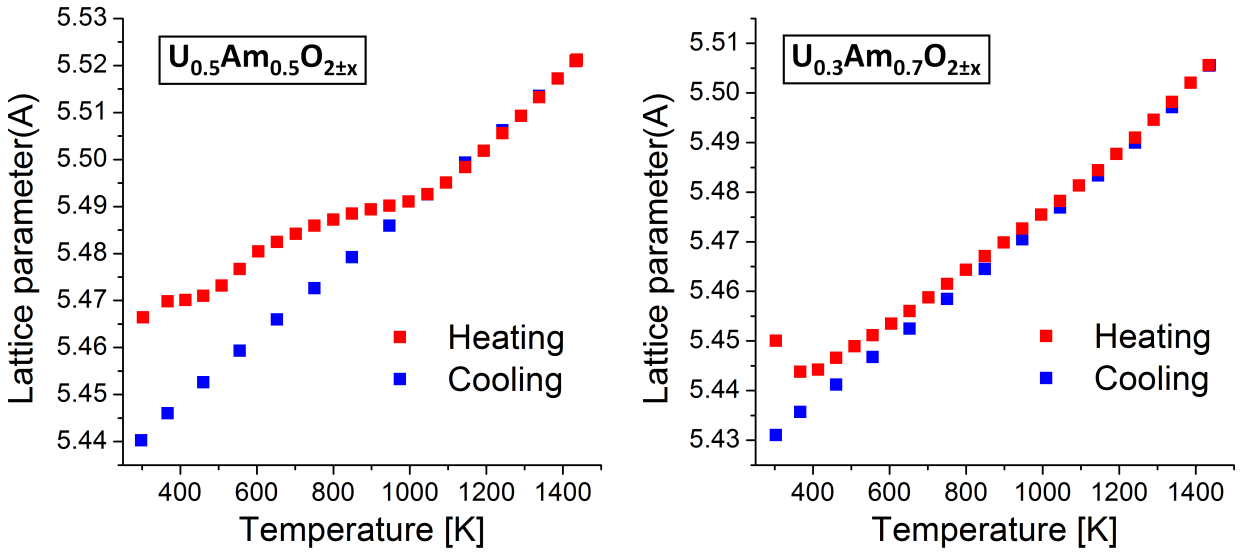

Figure 10: Lattice parameter variation as a function of temperature for Am50 and Am70 in air. (The lattice parameter uncertainty coincides with the symbol size).

the samples. Interestingly, for Am50, the lattice parameters obtained during the cooling overlapped those of the heating in the $1000 \lesssim T \lesssim 1473$ K temperature range. This indicates that the most significant variations of the composition occurred, during the heating, below 1000 K. From the subsequent lattice parameter evolution, one can suppose that the O/M ratio was constant for the rest of the thermal treatment. Similar conclusions can be drawn for Am70, with an overlapping of the heating/cooling lattice parameters for T$\gtrsim$ 700 K, indicating that the O/M variations, if any, occurred at even lower temperature for this sample.

3.3 Final room-temperature state

At the end of the thermal treatment in air, the samples were re-ground and then re-prepared for a XRD acquisition, in order to eliminate possible errors coming from the swelling, due to the M_3O_8 formation. The XRD patterns, shown in Fig. 11 for the biphasic samples, were refined according to the Rietveld method.[27] The orthorhombic *C2mm* structure was adopted for the room temperature M_3O_8 phase. The results are reported in Tab. 2.

The amount of M_3O_8 considerably decreases with the overall americium content of the

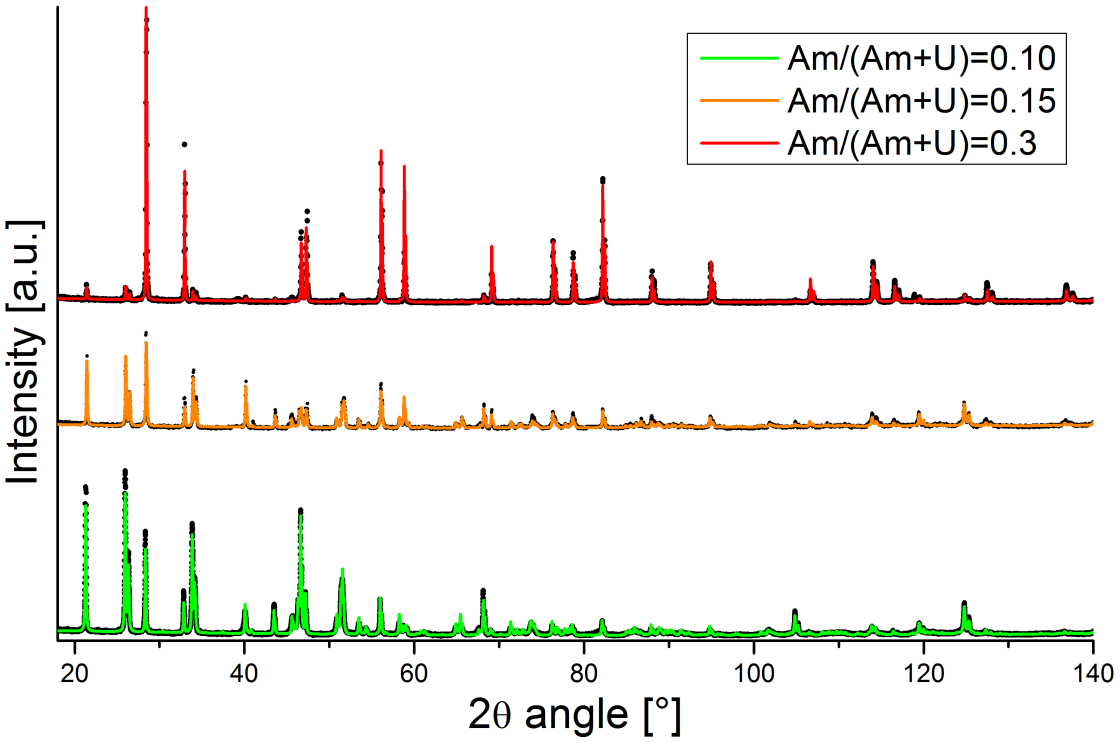

Figure 11: XRD data (black points) acquired at room temperature and Rietveld fits (colored curves), for the samples with overall Am/(Am+U) = 0.10, 0.15 and 0.28.

Table 2: Results of the Rietveld refinements at room temperature.

Am/(Am+U)	MO_{2+x}/M_4O_9 (Fm-3m)		M_3O_8 (C2mm)				R_{wp}
(at.%)	wt.%	a (Å)	wt.%	a (Å)	b (Å)	c (Å)	(%)
10	21(5)	5.430(3)	79(5)	6.733(3)	11.938(3)	4.147(3)	9.5
15	43(5)	5.434(2)	57(5)	6.725(3)	11.938(3)	4.145(3)	7.6
28	95(5)	5.432(2)	5(4)	6.726(3)	11.931	4.146	5.3
48	100	5.440(1)	0	-	-	-	5.1
67	100	5.431(1)	0	-	-	-	5.4

sample, passing from 79(5) wt.% for Am/(Am+U) = 0.10, to 57(5) wt.% for Am/(Am+U) = 0.15 and only 5(4) wt.% for Am/(Am+U) = 0.28. As already said, the M_3O_8 phase was not present in the Am50 and Am70 samples, which maintained the fluorite structure.

The lattice parameters found for the M_3O_8 structure are compared to those of α-U_3O_8[29] in Fig. 12, where the ratios a/a(U_3O_8), b/b(U_3O_8), c/c(U_3O_8) are represented. For the three samples, the obtained c lattice parameter is equal to that of U_3O_8 (c = 4.147 Å), in the uncertainty limit. On the contrary, small but significant differences were found for the a

and b parameters, respectively longer and shorter than those of U_3O_8 (a = 6.716 Å and b = 11.96 Å). On the basis of these systematic variations, the incorporation of slight quantities of americium in the *C2mm* structure can be supposed. Moreover, the a, b, c lattice parameters have very close values for the three samples. In the hypothesis of oxygen stoichiometric (O/M = 2.667, as in U_3O_8), this indicates that the M_3O_8 phases of the three samples had a very close Am/(Am+U) ratio. Finally, plotting the fraction of the cubic phase as a function of the overall americium content in the sample (Fig. 13), a linear trend can be observed and the zero-crossing of the line indicates a solubility of americium in the M_3O_8 structure around 5 at.%

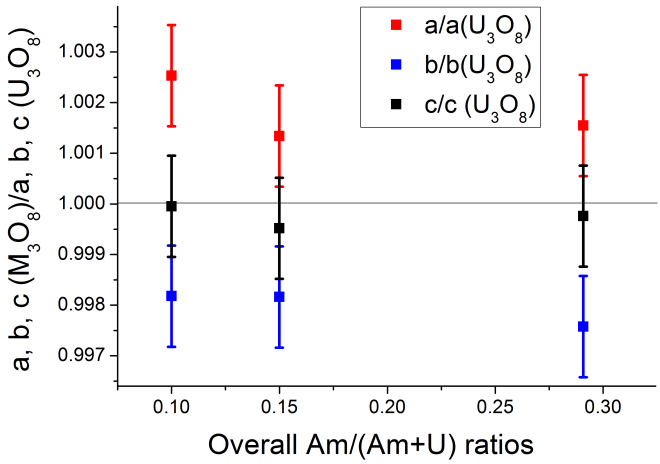

Figure 12: Ratios between the a, b, c lattice parameters of M_3O_8 (this work) and those of α-U_3O_8, for the three samples with overall Am/(Am+U) ratios = 0.10, 0.15 and 0.28.

4 Discussion

The UO_2 phase is stoichiometric at room temperature and the hyperstoichiometric domain (O/M > 2) exists only for T > 600 K, as shown in Fig. 4. As already mentioned, AmO_2 is the oxide with the highest O/M ratio in the Am-O system. Therefore, the extension of the hyperstoichiometric UO_2 domain to lower temperature with the adding of americium can be excluded. For the three mixed oxides, the MO_2 lattice parameter increased linearly

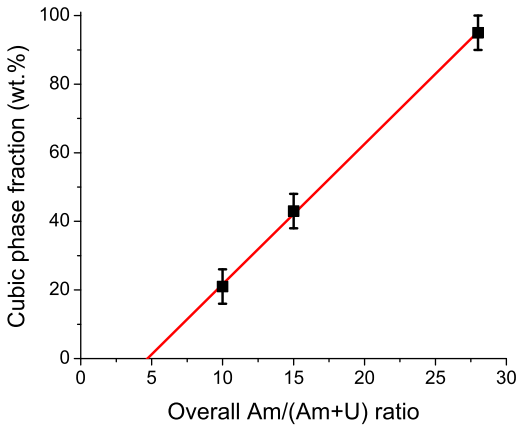

Figure 13: Weight fraction of the cubic phase (M_4O_9 or MO_{2+x}) as a function of the overall americium content.

at the beginning of the heating in air, confirming that no O/M increase is possible at low temperature. Subsequently, for Am/(Am+U) = 0.10 and 0.15, a rapid oxidation occurred for T $\simeq$ 520 K, with the formation of the M_4O_9 phase. On the contrary, the oxidation of the Am/(Am+U) = 0.28 started for T $\geq$ 600 K, in a slow way, consistently with the onset of a MO_{2+x} hyperstoichiometric domain. For Am/(Am+U) = 0.10 and 0.15, the oxidation proceeded with the entering of the M_4O_9+M_3O_8 biphasic domain, as for UO_2. However, the formation of these other oxides with O/M >2 was slowed down and limited by the addition of americium, in comparison to pure UO_2. In fact, the oxidation transitions were shifted toward higher temperatures and the final M_3O_8 content was lower and lower with the increasing of the overall Am/(Am+U) ratio. For Am/(Am+U) = 0.28, the oxidation proceeded with the MO_{2+x}+M_3O_8 equilibrium. This equilibrium could not be correctly represented in the path traced on the U-O phase diagram, in Fig. 4. Indeed, in the binary U-O system, the UO_{2+x}+U_3O_8 biphasic domain exists for T > 1400 K, whereas for lower temperatures the U_3O_8 appearance must occur through the U_4O_9 formation. On the contrary, for the Am/(Am+U) = 0.28 composition, the MO_{2+x}+M_3O_8 coexistence started at about 1000 K. This indicates that, for Am/(Am+U) $\simeq$ 0.30, the MO_{2+x}/M_3O_8 domain is extended at lower temperature, at the expense of the M_4O_9/M_3O_8 domain. The extent of the oxidation was

however very limited for this composition, with only 5±4 wt.% of M_3O_8, confirming that increasing the americium content hinders the formation of this phase.

It must be remarked that the transformation temperatures observed during the heating- summarized in Tab. 3- are interesting kinetic oxidation data, but they cannot be strictly associated to the phase diagram transition temperatures. The achievement of the thermo-

Table 3: Observed phase transitions and corresponding temperatures in air.

Overall	Transformation temperatures [K]			
Am/M	$MO_2 \rightarrow MO_{2+x}$	$MO_{2+x} \rightarrow M_4O_9$	α'-M_3O_8 formation	α'-$M_3O_8 \rightarrow$ α-M_3O_8
0.10	-	520(20)	650(50)	567(50)
0.15	-	535(20)	775(20)	530(50)
0.30	500-950	-	995(25)	460(50)
0.50	600-900	-	-	-
0.70	-	-	-	-

dynamic equilibrium cannot be assured during the heating. On the contrary, for all the samples analysed, no evolution was observed during the 4-hours isothermal measurement at 1470 K and, hence, it can be concluded that the oxides were at their thermodynamic equilibrium. Moreover, as previously discussed, the lattice parameter evolution during the cooling indicated that the composition was mostly constant. Indeed, the lattice parameters of the cubic phases (both MO_{2+x} and M_4O_9) decreased with a regular, linear evolution and they could be fitted as a linear function of the temperature:

$$a(T) = a_{RT} + b \cdot (T - 298.15). \tag{1}$$

The parameters of Eq. (1), for each sample, are reported in Tab. 4.

In particular, it must be underlined that no rupture in the lattice trend of the cubic structure was observed when the M_3O_8 phase transformed from hexagonal to orthorhombic (460-570 K). This indicates that there was no a interdiffusion of uranium or americium between the MO_2 and the M_3O_8 phases during this transformation. As previously observed,

Table 4: Parameters of Eq. (1) for the lattice parameter expansion of the cubic phase in air.

Overall Am/(Am+U)	Phase	a_{RT} [Å]	b $\cdot 10^{-5}$ [Å·K^{-1}]
0.10	M_4O_9	5.430(3)	5.6(8)
0.15	M_4O_9	5.434(2)	5.9(8)
0.28	MO_{2+x}	5.432(2)	7.3(5)
0.48	$MO_{2\pm x}$	5.440(1)	6.9(4)
0.67	$MO_{2\pm x}$	5.431(1)	6.5(4)

the lattice parameters of the *C2mm* structure were close for the three compositions and with systematic differences in comparison to the α-U_3O_8. This suggests an incorporation of americium in this structure, similar for the three samples, here estimated around 5 at.%. This is in disagreement with the previous results of Caisso *et al.*,[14] who obtained a monophasic $(U_{0.9}Am_{0.1})_3O_8$ oxide through a wet chemical route based on the use of ion-exchange resin microspheres. In that study, the authors observed the hexagonal *P-62m* structure at room temperature and they suggested a stabilization of this form through the incorporation of americium. Here, the sample with Am/(Am+U) = 0.10 was biphasic. Moreover, as already said, no effect on the cubic phases (M_4O_9 and MO_{2+x}) was observed during the α'-$M_3O_8 \rightarrow \alpha$-$M_3O_8$ transition. Therefore, the composition of M_3O_8 was necessarily constant during the structural change. This indicates that the solubility of americium is likely equal for both the hexagonal and orthorhombic M_3O_8 polymorphs. Therefore, the results of this work contrast with the stabilization of the hexagonal structure and points toward a lower solubility, around 5 at.%. In the study of Caisso *et al*,[14] the M_3O_8 sample was obtained by calcination at 973 K of ion exchange resin microspheres. It can be supposed that, at that relatively low temperature, actinide mobilities are low and the synthesis route adopted by Caisso *et al.* can induce an over-saturation of M_3O_8 in americium. This over-saturation could be the cause for the stabilization of the hexagonal phase, which would explain why the transition toward the orthorhombic structure was not observed in that work.[14]

5 Conclusions and perspectives

In this work, the oxidation in air of (U,Am)$O_{2\pm x}$ oxides has been investigated by HT-XRD. The results showed a complex behaviour, strongly dependent on the americium content of the solid solution.

The $MO_2 \rightarrow M_4O_9$ transition occurred for the Am/M = 0.10 and 0.15 compositions, at ∼520 and ∼535 K, respectively. This transition was identified by its rapidity (∼ 30 minutes) and the simultaneous presence of two cubic structures (MO_{2+x} and M_4O_9).

Slow $MO_2 \rightarrow MO_{2+x}$ oxidation, spread across wide temperature ranges (500-950 K) was instead observed for Am/M = 0.28 and, in minor extent, for Am/M = 0.48 and 0.67. These features indicated a smaller increase of the O/M ratio for the MO_{2+x} phase.

The M_3O_8 phase was observed only for the samples with Am/M ≤ 0.28, whereas the Am/M = 0.48 and 0.67 compositions remained single-phase cubic. The temperature of the M_3O_8 appearance increased with the americium content, from 650(20) K for Am/M = 0.10, up to 995(25) K for Am/M = 0.28. The total amount of this phase at room temperature decreased with the overall americium content of the sample, from 79(5) wt.% for Am/M=0.10 to only 5(4) wt.% for Am/M = 0.28. These results clearly indicate that the americium hinders the formation of *hyperstoichiometric* oxides. This is consistent with the behaviour already observed for mixed U-Np oxides[21] and U-Pu oxides,[34] but the effect is even more accentuated with americium, confirming a trend along the actinide series. Two M_3O_8 polymorphs were observed: the hexagonal *P-62m* phase transformed into the orthorhombic *C2mm* during the cooling. This transition occurred at T = 567(50), 530(50) and 460(50) K for the samples with overall Am/M = 0.10, 0.15, 0.28, respectively. No rupture in the lattice parameter trend of the cubic phase was observed at this temperature, indicating that there was not a further repartition of uranium and americium during this transformation. From one side, this allowed obtaining important structural data on the lattice parameter expansion with temperature of the MO_{2+x} phase. On the other side, the americium solubility in M_3O_8 was estimated to 5 at.% from XRD refinements of the room temperature data, in both the

observed M_3O_8 structures. In a future work, further investigations will be performed on the oxidized samples, in order to precisely determine their final compositions, to confirm the americium solubility in M_4O_9 and M_3O_8 and to obtain precise phase diagram data.

Data availability statement

Additional data can be provided on request.

References

(1) D'Agata, E.; Hania, P. R.; Bejaoui, S.; Sciolla, C.; Wyatt, T.; Hannink, M. H. C.; Herlet, N.; Jankowiak, A.; Klaassen, F. C.; Lapetite, J. M.; Boomstra, D. A.; Phelip, M.; Delage, F. The results of the irradiation experiment MARIOS on americium transmutation. *Annals of Nuclear Energy* **2013**, *62*, 40–49.

(2) Inoue, M. Thermal conductivity of uranium–plutonium oxide fuel for fast reactors. *Journal of Nuclear Materials* **2000**, *282*, 186–195.

(3) Kato, M.; Segawa, T.; Takeuchi, K.; Kashimura, M.; Kihara, Y. Development of an advanced fabrication process for fast reactor MOX fuel. **2009**,

(4) Viswanathan, R. Fuel clad chemical interactions in fast reactor MOX fuels. *Journal of Nuclear Materials* **2014**, *444*, 101–111.

(5) Calabrese, R.; Manara, D.; Schubert, A.; van de Laar, J.; Van Uffelen, P. Melting temperature of MOX fuel for FBR applications: TRANSURANUS modelling and experimental findings. *Nuclear Engineering and Design* **2015**, *283*, 148–154.

(6) Prieur, D.; Jankowiak, A.; Delahaye, T.; Herlet, N.; Dehaudt, P.; Blanchart, P. Fabrication and characterisation of U0.85Am0.15O2-x discs for MARIOS irradiation program. *Journal of Nuclear Materials* **2011**, *414*, 503–507.

(7) Lebreton, F.; Horlait, D.; Caraballo, R.; Martin, P. M.; Scheinost, A. C.; Rossberg, A.; Jégou, C.; Delahaye, T. Peculiar Behavior of (U,Am)O2-x Compounds for High Americium Contents Evidenced by XRD, XAS, and Raman Spectroscopy. *Inorg. Chem.* **2015**, *54*, 9749–9760.

(8) Prieur, D.; Martin, P. M.; Jankowiak, A.; Gavilan, E.; Scheinost, A. C.; Herlet, N.; Dehaudt, P.; Blanchart, P. Local Structure and Charge Distribution in Mixed Uranium–Americium Oxides: Effects of Oxygen Potential and Am Content. *Inorg. Chem.* **2011**, *50*, 12437–12445.

(9) Prieur, D.; Martin, P.; Lebreton, F.; Delahaye, T.; Banerjee, D.; Scheinost, A. C.; Jankowiak, A. Accommodation of multivalent cations in fluorite-type solid solutions: Case of Am-bearing UO2. *Journal of Nuclear Materials* **2013**, *434*, 7–16.

(10) Prieur, D.; Lebreton, F.; Caisso, M.; Martin, P. M.; Scheinost, A. C.; Delahaye, T.; Manara, D. Melting behaviour of americium-doped uranium dioxide. *The Journal of Chemical Thermodynamics* **2016**, *97*, 244–252.

(11) Epifano, E.; Beneš, O.; Vălu, O. S.; Zappey, J.; Lebreton, F.; Martin, P. M.; Guéneau, C.; Konings, R. J. M. High temperature heat capacity of (U, Am)O2±x. *Journal of Nuclear Materials* **2017**, *494*, 95–102.

(12) Epifano, E.; Naji, M.; Manara, D.; Scheinost, A. C.; Hennig, C.; Lechelle, J.; Konings, R. J. M.; Guéneau, C.; Prieur, D.; Vitova, T.; Dardenne, K.; Rothe, J.; Martin, P. M. Extreme multi-valence states in mixed actinide oxides. *Communications Chemistry* **2019**, *2*, 59.

(13) Bartscher, W.; Sari, C. A thermodynamic study of the uranium-americium oxide U0.5Am0.5O2. *Journal of Nuclear Materials* **1983**, *118*, 220–223.

(14) Caisso, M.; Roussel, P.; Den Auwer, C.; Picart, S.; Hennig, C.; Scheinost, A. C.; De-

lahaye, T.; Ayral, A. Evidence of Trivalent Am Substitution into U3O8. *Inorg. Chem.* **2016**, *55*, 10438–10444.

(15) Epifano, E.; Prieur, D.; Martin, P. M.; Guéneau, C.; Dardenne, K.; Rothe, J.; Vitova, T.; Dieste, O.; Wiss, T.; Konings, R. J. M.; Manara, D. Melting behaviour of uranium-americium mixed oxides under different atmospheres. *The Journal of Chemical Thermodynamics* **2020**, *140*, 105896.

(16) Guéneau, C.; Dupin, N.; Sundman, B.; Martial, C.; Dumas, J.-C.; Gossé, S.; Chatain, S.; Bruycker, F. D.; Manara, D.; Konings, R. J. M. Thermodynamic modelling of advanced oxide and carbide nuclear fuels: Description of the U–Pu–O–C systems. *Journal of Nuclear Materials* **2011**, *419*, 145–167.

(17) Allen, G. C.; Tempest, P. A.; Tyler, J. W. Oxidation of crystalline UO2 studied using X-ray photoelectron spectroscopy and X-ray diffraction. *J. Chem. Soc., Faraday Trans. 1* **1987**, *83*, 925–935.

(18) McEachern, R. J.; Taylor, P. A review of the oxidation of uranium dioxide at temperatures below 400°C. *Journal of Nuclear Materials* **1998**, *254*, 87–121.

(19) Rousseau, G.; Desgranges, L.; Charlot, F.; Millot, N.; Nièpce, J. C.; Pijolat, M.; Valdivieso, F.; Baldinozzi, G.; Bérar, J. F. A detailed study of UO2 to U3O8 oxidation phases and the associated rate-limiting steps. *Journal of Nuclear Materials* **2006**, *355*, 10–20.

(20) Desgranges, L.; Baldinozzi, G.; Rousseau, G.; Nièpce, J.-C.; Calvarin, G. Neutron Diffraction Study of the in Situ Oxidation of UO2. *Inorg. Chem.* **2009**, *48*, 7585–7592.

(21) Chollet, M.; Belin, R. C.; Richaud, J.-C.; Reynaud, M.; Adenot, F. High-Temperature X-ray Diffraction Study of Uranium–Neptunium Mixed Oxides. *Inorg. Chem.* **2013**, *52*, 2519–2525.

(22) Epifano, E.; Guéneau, C.; Belin, R. C.; Vauchy, R.; Lebreton, F.; Richaud, J.-C.; Joly, A.; Valot, C.; Martin, P. M. Insight into the Am–O Phase Equilibria: A Thermodynamic Study Coupling High-Temperature XRD and CALPHAD Modeling. *Inorganic Chemistry* **2017**, *56*, 7416–7432.

(23) Rostaing, C.; Poinssot, C.; Warin, D.; Baron, P.; Lorraina, B. Development and Validation of the EXAm Separation Process for Single Am Recycling. *Procedia Chemistry* **2012**, *7*, 367–373.

(24) Delahaye, T.; Lebreton, F.; Horlait, D.; Herlet, N.; Dehaudt, P. Application of the UMACS process to highly dense U1-xAmxO2 MABB fuel fabrication for the DIAMINO irradiation. *Journal of Nuclear Materials* **2013**, *432*, 305–312.

(25) Vauchy, R.; Belin, R. C.; Richaud, J.-C.; Valenza, P. J.; Adenot, F.; Valot, C. Studying radiotoxic materials by high temperature X-ray diffraction. *Applied Materials Today* **2016**, *3*, 87–95.

(26) Pawley, G. S. Unit-cell refinement from powder diffraction scans. *J Appl Crystallogr* **1981**, *14*, 357–361.

(27) Rietveld, H. M. A profile refinement method for nuclear and magnetic structures. *J Appl Crystallogr* **1969**, *2*, 65–71.

(28) Bruker AXS: Madison, WI, *TOPAS V4: General Profile and Structure Analysis Software for Powder Diffraction Data. User's Manual.*; 2005.

(29) Ackermann, R. J.; Chang, A. T.; Sorrell, C. A. Thermal expansion and phase transformations of the U3O8-z phase in air. *Journal of Inorganic and Nuclear Chemistry* **1977**, *39*, 75–85.

(30) Loopstra, B. O. On the crystal structure of alpha-U3O8. *Journal of Inorganic and Nuclear Chemistry* **1977**, *39*, 1713–1714.

(31) Loopstra, B. O. The structure of beta-U3O8. *Acta Crystallographica Section B Structural Crystallography and Crystal Chemistry* **1970**, *26*, 656–657.

(32) Horlait, D.; Lebreton, F.; Roussel, P.; Delahaye, T. XRD Monitoring of Self-Irradiation in Uranium–Americium Mixed Oxides. *Inorg. Chem.* **2013**, *52*, 14196–14204.

(33) Lebreton, F. *Synthèse et caractérisation d'oxydes mixtes d'uranium et d'américium*; Limoges, 2014.

(34) Strach, M.; Belin, R. C.; Richaud, J.-C.; Rogez, J. High Temperature X-ray Diffraction Study of the Oxidation Products and Kinetics of Uranium–Plutonium Mixed Oxides. *Inorg. Chem.* **2014**, *53*, 12757–12766.